Supplementary Information

# Incorporation of multiple supramolecular binding sites into a robust MOF for benchmark one-step ethylene purification

Enyu Wu[1+], Xiao-Wen Gu[1+], Di Liu[1], Xu Zhang[2], Hui Wu[3], Wei Zhou[3], Guodong Qian[1] and Bin Li[1]*

[1] State Key Laboratory of Silicon and Advanced Semiconductor Materials, School of Materials Science and Engineering, Zhejiang University, Hangzhou 310027, China.

[2] School of Chemistry and Chemical Engineering, Huaiyin Normal University, Huaian 223300, China.

[3] NIST Center for Neutron Research, National Institute of Standards and Technology, Gaithersburg, MD 20899-6102, USA.

[+] These authors contributed equally to this work.

*E-mail: bin.li@zju.edu.cn

**Table of Contents**

## Supplementary Notes

### IAST calculations

The IAST was used to predict the binary mixture adsorption from the experimental pure gas isotherms. To perform the integrations required by IAST, single-component isotherms should be fitted by the correct model. The experimental pure component isotherm data for $C_2H_2$, $C_2H_6$ and $C_2H_4$ in Al-PyDC measured at 296 K were fitted with single-site Langmuir-Freundlich equation.

$$q = q_{\text{sat}} \frac{bp^v}{1+bp^v} \tag{1}$$

with T-dependent parameters $b$

$$b = b_0 \exp\left(\frac{E}{RT}\right) \tag{2}$$

Here, $p$ is the pressure of the bulk gas in equilibrium with the adsorbed phase (kPa), $q$ is the amount adsorbed per mass of adsorbent (mmol $g^{-1}$), $q_{\text{sat}}$ is the saturation capacities of site 1 (mmol $g^{-1}$), $b$ is the affinity coefficients of site 1 ($kPa^{-1}$) and $v$ represents the deviations from an ideal homogeneous surface. The fitted parameter values are presented in Supplementary Table 2.

The fitted parameters were then used to predict multi-component adsorption with IAST. The selectivity of preferential adsorption of component 1 over component 2 in a mixture containing 1 and 2, can be formally defined as:

$$S_{\text{ads}} = \frac{q_1/q_2}{p_1/p_2} \tag{3}$$

In equation (3), $q_1$ and $q_2$ are the molar loadings of the adsorbed phase in equilibrium with the bulk gas phase with partial pressures $p_1$ and $p_2$. IAST calculations of the adsorption selectivity for 1/99 (v/v) $C_2H_2/C_2H_4$ and 50/50 (v/v) $C_2H_6/C_2H_4$ mixtures in Al-PyDC at 296 K are shown in Fig. 3c.

### Isosteric heat of adsorption

A virial-type expression of comprising the temperature-independent parameters $a_i$ and $b_j$ was employed to calculate the enthalpies of adsorption for $C_2H_2$, $C_2H_4$ and $C_2H_6$ on Al-PyDC. In each case, the data were fitted with equation:

$$\ln P = \ln N + 1/T \sum_{i=0}^{m} a_i N_i + \sum_{j=0}^{n} b_j N_j \tag{4}$$

Here, $P$ is the pressure expressed in Pa, $N$ is the amount absorbed in mmol $g^{-1}$, $T$ is the temperature in K, $a_i$ and $b_j$ are virial coefficients, and $m$, $n$ represent the number of coefficients required to adequately describe the isotherms ($m$ and $n$ were gradually increased till the contribution of extra added $a$ and $b$ coefficients was deemed to be statistically insignificant towards the overall fit. The average value of the squared deviations from the experimental values was minimized). The values of the virial coefficients $a_0$ to $a_m$ were then used to calculate the isosteric heat of adsorption utilizing the following expression:

$$Q_{st} = -R \sum_{i=0}^{m} a_i N_i \quad (5)$$

$Q_{st}$ is the coverage-dependent isosteric heat of adsorption and $R$ is the universal gas constant. The heat enthalpies of $C_2H_2$, $C_2H_6$ and $C_2H_4$ sorption for Al-PyDC in this manuscript are determined by using the sorption data measured in the pressure range from 0 to 1 bar (at 273 K, 296 K and 313 K).

**Supplementary Discussion**

**$C_2$ adsorption at different temperatures**

Since the $C_2H_2$ and $C_2H_6$ binding affinity are stronger than $C_2H_4$ (Supplementary Fig. 12), it is normal that the $C_2H_2$ and $C_2H_6$ uptakes of Al-PyDC are higher than that of $C_2H_4$ at different temperatures. As shown in Fig. 3b and Supplementary Fig. 5, Al-PyDC indeed exhibits more obviously preferential adsorption of $C_2H_2$ (8.24 and 5.80 mmol $g^{-1}$ at 1 bar) and $C_2H_6$ (4.20 and 3.02 mmol $g^{-1}$) over $C_2H_4$ (3.44 and 2.65 mmol $g^{-1}$) at 296 K and 313 K. However, at 273 K, the $C_2H_4$ and $C_2H_6$ uptakes (5.0 and 5.13 mmol $g^{-1}$) are quite similar at 1 bar, accompanied with the preferential adsorption of $C_2H_6$ over $C_2H_4$ at low-pressure regions. To explain this abnormal behavior between $C_2H_6$ and $C_2H_4$ at 273 K, our gas-loaded crystal structures experimentally revealed that the main binding sites for $C_2H_6$ and $C_2H_4$ are the same but with different binding strength (Figs. 4e and 4f). The full occupancy of these main binding sites corresponds to the saturated adsorption amount of 5.08 mmol $g^{-1}$. At 273 K, the quite similar $C_2H_6$ and $C_2H_4$ uptakes (5.0 and 5.13 mmol $g^{-1}$) are consistent well with the saturated amount obtained from gas-loaded crystal structures. This indicates that the main binding sites are fully occupied for both $C_2H_4$ and $C_2H_6$ at 273 K. With the adsorption temperature increased to 296

K or 313 K, the adsorption occupancy of the main binding sites would be reduced for all $C_2$ gases; however, the stronger binding affinity of $C_2H_6$ results in a higher adsorption occupancy of the main binding sites than $C_2H_4$ (82% vs 68% at 296 K, and 59% vs 52% at 313 K). The same situation was also observed for $C_2H_2$ adsorption, in which $C_2H_2$ uptake at 273 K (10.34 mmol $g^{-1}$) matches with the full occupation of the main binding sites (10.1 mmol $g^{-1}$) obtained by $C_2H_2$-loaded crystal structure. With the temperature increased to 296 and 313 K, the adsorption occupancy of the main binding sites was decreased to be 82% at 296 K and 58% at 313 K. Such stronger binding affinity to result in higher adsorption occupancy of the main binding sites was also exemplified in other materials for reversed $C_2H_4/C_2H_6$ separation.[1]

Therefore, the similar $C_2H_6$ and $C_2H_4$ uptakes at 273 K are mainly dominated by the full occupancy of the main binding sites for both gases. With the adsorption temperature increased to 296 K and 313 K, the stronger binding affinity of $C_2H_6$ enables a higher adsorption occupancy of the main binding sites than $C_2H_4$, thus resulting in the more obviously preferential adsorption of $C_2H_6$ over $C_2H_4$ at 296 K and 313 K than at 273 K.

## Notation

| | |
|---|---|
| $q$ | Component molar loading of species $i$, mol kg$^{-1}$ |
| $q_{sat}$ | Saturation loading, mol kg$^{-1}$ |
| $b$ | Langmuir-Freundlich constant, kPa$^{-v}$ |
| $T$ | Absolute temperature, K |
| $a_i$ | Virial coefficients, dimensionless |
| $b_j$ | Virial coefficients, dimensionless |
| $Q_{st}$ | Isosteric heat of adsorption, kJ mol$^{-1}$ |

## Greek letters

| | |
|---|---|
| $v$ | Freundlich exponent, dimensionless |

**Supplementary Tables**

**Supplementary Table 1.** Physical properties of $C_2H_2$, $C_2H_4$, and $C_2H_6$.

| Molecular formula | Molecular dimension (Å) | | | Kinetic diameter (Å) | Polari × $10^{-25}$ ($cm^{-3}$) | Boiling point (K) |
|---|---|---|---|---|---|---|
| | *X* | *Y* | *Z* | | | |
| $C_2H_2$ | 3.32 | 3.34 | 5.70 | 3.33 | 33.3−33.9 | 188.4 |
| $C_2H_4$ | 3.28 | 4.18 | 4.84 | 4.16 | 42.5 | 169.4 |
| $C_2H_6$ | 3.81 | 4.08 | 4.82 | 4.44 | 44.3−44.7 | 184.6 |

**Supplementary Table 2.** Single-site Langmuir-Freundlich parameter fits for $C_2H_2$, $C_2H_4$ and $C_2H_6$ in Al-PyDC. The fits are based on experimental isotherm data at 296 K.

| | $q_{sat}$ mol $kg^{-1}$ | *b* $kPa^{-v}$ | *v* dimensionless |
|---|---|---|---|
| $C_2H_2$ | 14.09674 | 6.20419 | 6.37767 |
| $C_2H_4$ | 0.023 | 0.01372 | 0.0255 |
| $C_2H_6$ | 0.87198 | 1.00448 | 0.92349 |

**Supplementary Table 3.** Summary of adsorption and separation metrics of $C_2H_2/C_2H_6$-selective materials reported in the literatures at 1 bar and room temperature.

| MOFs | $C_2H_2$ uptake[a] (mmol $g^{-1}$) | $C_2H_6$ uptake[a] (mmol $g^{-1}$) | $C_2H_2/C_2H_4$ selectivity[b] | $C_2H_6/C_2H_4$ selectivity[c] | Ref. |
|---|---|---|---|---|---|
| **Al-PyDC** | **8.24** | **4.20** | **4.3** | **1.9** | **This work** |
| Zn(ad)(int) | 2.90 | 2.32 | 1.61 | 2.4 | 2 |
| $CuTiF_6$-TPPY | 3.62 | 2.82 | 5.03 | 2.12[e] | 3 |
| Zn(BDC)($H_2$BPZ) | 4.46 | 3.60 | 1.6[d] | 2.2 | 4 |
| UiO-67-$(NH_2)_2$ | 5.90 | 5.32 | 2.1 | 1.7 | 5 |
| NPU-1 | 5.09 | 4.50 | 1.4[d] | 1.32 | 6 |
| NPU-2 | 4.02 | 4.43 | 1.25[d] | 1.52 | 6 |
| TJT-100 | 4.46 | 3.75 | 1.8 | 1.2[f] | 7 |
| Azole-Th-1 | 3.62 | 4.47 | 1.0 | 1.46 | 8 |
| NUM-9 | 2.36 | 2.47 | 1.47 | 1.62 | 9 |
| UPC-612 | 3.01 | 3.57 | 1.07[e] | 1.41 | 10 |
| UPC-613 | 2.83 | 2.54 | 1.4[e] | 1.47 | 10 |
| MOF-525 | 2.64 | 2.70 | 1.44[e] | 1.25 | 10 |
| MOF-525(Co) | 2.62 | 2.21 | 1.87[e] | 1.1 | 10 |
| Ag-PCM-102 | 4.59 | 3.69 | 1.5 | – | 11 |

[a] At 1 bar and room temperature.

[b] IAST selectivity for 1/99 $C_2H_2/C_2H_4$ gas mixture.

[c] IAST selectivity for 50/50 $C_2H_6/C_2H_4$ gas mixture.

[d] Selectivity is for a 50/50 mixture.

[e] Selectivity is for a 10/90 mixture.

[f] Selectivity is for a 1/99 mixture.

**Supplementary Table 4.** Crystallographic data and structure refinement results of $C_2H_2$-loaded Al-PyDC, $C_2H_4$-loaded Al-PyDC, $C_2H_6$-loaded Al-PyDC and Al-PyDC-hydrated.

| Unit cell parameters | $C_2H_2$@Al-PyDC | $C_2H_4$@Al-PyDC | $C_2H_6$@Al-PyDC | Al-PyDC-hydrated |
|---|---|---|---|---|
| Formula | $C_{20}H_{16}Al_2N_2O_{10}$ | $C_{16}H_{16}Al_2N_2O_{10}$ | $C_{16}H_{20}Al_2N_2O_{10}$ | $C_{24}H_{49}Al_4N_4O_{38}$ |
| Formula weight | 498.31 | 450.27 | 454.30 | 1109.59 |
| Temperature/K | 200(2) | 200(2) | 200(2) | 170(2) |
| Crystal system | Tetragonal | Tetragonal | Tetragonal | Tetragonal |
| Space group | $I4_1/amd$ | $I4_1/amd$ | $I4_1/amd$ | $I4_1md$ |
| $a$, $b$ (Å) | 21.2209(11) | 21.198(3) | 21.2349(11) | 21.1895(3) |
| $c$ (Å) | 10.6352(15) | 10.675(4) | 10.6874(11) | 10.6283(3) |
| $\alpha$ (°) | 90 | 90 | 90 | 90 |
| $\beta$ (°) | 90 | 90 | 90 | 90 |
| $\gamma$ (°) | 90 | 90 | 90 | 90 |
| $V$ (Å$^3$) | 4789.3(8) | 4797(2) | 4819.2(7) | 4772.05(19) |
| $Z$ | 8 | 8 | 8 | 4 |
| $D_{calcd}$ (g cm$^{-3}$) | 1.382 | 1.247 | 1.252 | 1.544 |
| $\mu$ (mm$^{-1}$) | 1.609 | 1.547 | 1.540 | 1.954 |
| $F$(000) | 2048 | 1856 | 1888 | 2308 |
| GOF | 1.115 | 1.044 | 1.066 | 1.060 |
| $R_{int}$ | 0.2574 | 0.3459 | 0.3499 | 0.1597 |
| $R_1$, $wR_2$ [I>=2σ (I)] | 0.1308, 0.3769 | 0.1644, 0.4952 | 0.1322, 0.3891 | 0.0545, 0.1462 |
| $R_1$, $wR_2$ [all data] | 0.1944, 1.106 | 0.2788, 1.037 | 0.1791, 2.791 | 0.0721, 1.059 |
| Largest diff. peak and hole (e Å$^{-3}$) | 0.578 and -0.656 | 1.077 and -0.423 | 1.012 and -0.607 | 0.939 and -0.702 |
| CCDC number | 2242152 | 2242153 | 2242154 | 2242155 |

**Supplementary Table 5.** The interactions between the $C_2H_2$ molecule and host framework in Al-PyDC, determined by $C_2H_2$-loaded single-crystal X-ray diffraction studies.

| | | | D···A (Å)[a] | H···A (Å)[b] |
|---|---|---|---|---|
| $C_2H_2$ | Site I | C−H···O | 3.24 | 2.47 |
| | | | 3.24 | 2.47 |
| | | | 3.44 | 3.13 |
| | | | 3.44 | 3.13 |
| | | | 3.36 | 3.30 |
| | | | 3.36 | 3.30 |
| | | O−H···C | 2.90 | 1.98 |
| | | | 2.90 | 1.98 |
| | | $C-H_{pyrrole}\cdots C_{C2H2}$ | 3.26 | 2.40 |
| | | | 3.26 | 2.40 |
| | Site II | C−H···O | 3.36 | 2.41 |
| | | | 3.73 | 3.12 |
| | | | 3.91 | 3.35 |
| | | N−H···C | 3.01 | 2.32 |
| | | | 3.30 | 2.88 |
| | | C−H···π | 4.10 | 3.18 |
| | Cluster | $C-H_{C2H2}\cdots C_{C2H2}$ | 4.09 | 3.78 |
| | | | 4.50 | 3.98 |
| | | | 4.50 | 4.40 |
| | | | 4.91 | 4.40 |

[a] The distance between the donor atom and the acceptor atom. [b] The distance between the hydrogen atom and the acceptor atom.

**Supplementary Table 6.** The interactions between the $C_2H_6$ molecule and host framework in Al-PyDC, determined by $C_2H_6$-loaded single-crystal X-ray diffraction studies..

| | | D···A (Å)[a] | H···A (Å)[b] |
|---|---|---|---|
| $C_2H_6$ | C−H···O | 4.32 | 3.54 |
| | | 4.32 | 3.54 |
| | | 4.76 | 4.08 |
| | | 4.76 | 4.08 |
| | | 4.43 | 4.36 |
| | | 4.43 | 4.36 |
| | | 5.12 | 4.37 |
| | | 5.12 | 4.37 |
| | | 4.72 | 4.42 |
| | | 4.72 | 4.42 |
| | | 5.41 | 4.51 |
| | | 5.41 | 4.51 |
| | | 5.60 | 4.65 |
| | | 5.60 | 4.65 |
| | C−H···N | 4.16 | 3.80 |
| | | 4.16 | 3.80 |
| | | 4.74 | 4.18 |
| | C−H···π | 4.07 | 3.33 |
| | | 4.07 | 3.33 |
| | | 4.35 | 3.71 |
| | | 4.35 | 3.71 |

[a] The distance between the donor atom and the acceptor atom. [b] The distance between the hydrogen atom and the acceptor atom.

**Supplementary Table 7.** The interactions between the $C_2H_4$ molecule and host framework in Al-PyDC, determined by $C_2H_4$-loaded single-crystal X-ray diffraction studies..

| | | D···A (Å)[a] | H···A (Å)[b] |
|---|---|---|---|
| $C_2H_4$ | C−H···O | 4.37 | 3.78 |
| | | 4.37 | 3.78 |
| | | 4.56 | 3.83 |
| | | 4.56 | 3.83 |
| | | 4.17 | 3.91 |
| | | 4.17 | 3.91 |
| | | 4.53 | 4.08 |
| | | 4.53 | 4.08 |
| | C−H···N | 4.04 | 3.21 |
| | | 4.17 | 3.42 |
| | C−H···π | 4.54 | 4.26 |
| | | 4.54 | 4.26 |

[a] The distance between the donor atom and the acceptor atom. [b] The distance between the hydrogen atom and the acceptor atom.

**Supplementary Table 8.** Comparison of stability and synthetic conditions of Al-PyDC with reported $C_2H_2/C_2H_6$-selective MOFs and other representative stable MOFs.

| | MOFs | Stability | | | Synthetic conditions | | | Ref. |
|---|---|---|---|---|---|---|---|---|
| | | Water | pH=1 | pH=12 | Temp (°C) | Time (h) | Solvent | |
| $C_2H_2/C_2H_6$-selective MOFs | **Al-PyDC** | √ | √ | √ | **85** | **9** | **$H_2O$** | **This work** |
| | Zn(ad)(int) | √ | –[a] | – | 120 | 72 | DMF | 3 |
| | Zn(BDC)($H_2$BPZ) | – | – | – | 120 | 576 | DMF | 4 |
| | UiO-67-$(NH_2)_2$ | √ | – | √ | 120 | 48 | DMF | 5 |
| | NPU-1 | – | – | – | 100 | 240 | DMA | 6 |
| | TJT-100 | √ | – | √ | 150 | 72 | DMF/$H_2O$ | 7 |
| | Azole-Th-1 | √ | √ | √ | 110 | 72 | DMF | 8 |
| | NUM-9 | – | – | – | 100 | 72 | DMA/EtOH/$H_2O$ | 9 |
| | UPC-612 | √ | √ | √ | 120 | 48 | DMF | 10 |
| | MOF-525 | – | – | – | 120 | 48 | DMF | 10 |
| Stable MOFs | MIL-53(Al) | √ | – | √ | 220 | 72 | $H_2O$ | 12 |
| | UiO-66 | √ | √ | √ | 120 | 24 | DMF | 13 |
| | ZIF-8 | √ | – | √ | 140 | 24 | DMF | 14 |
| | MIL-101(Cr) | √ | √ | √ | 220 | 8 | $H_2O$ | 15 |
| | PCN-250 | √ | √ | √ | 140 | 12 | DMF | 16 |
| | BUT-12 | √ | √ | – | 120 | 48 | DMF | 17 |

[a] Stability in the corresponding conditions was not reported in literatures.

## Supplementary Figures

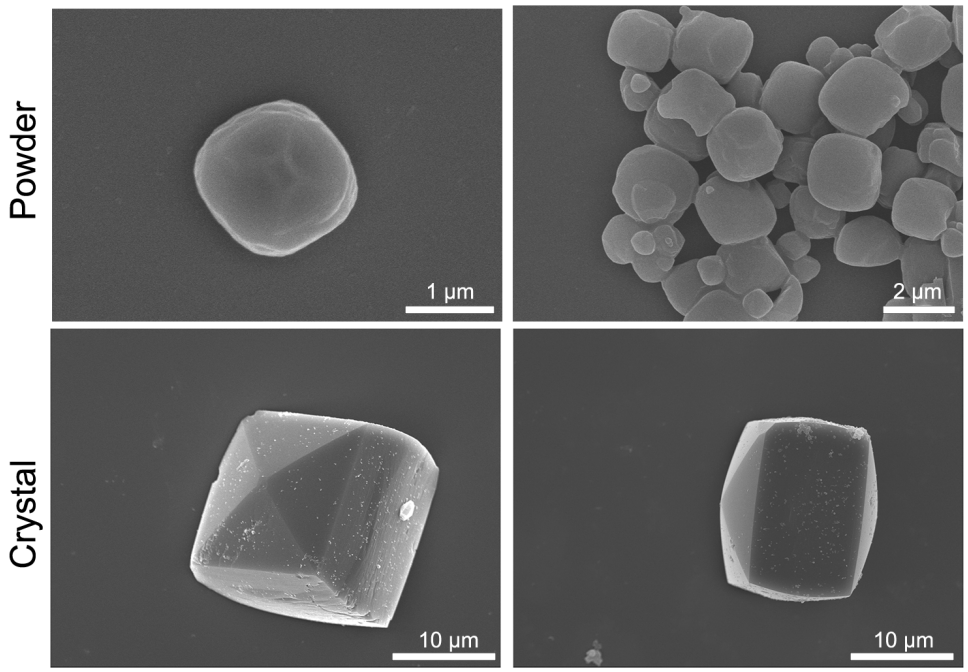


**Supplementary Fig. 1 SEM images.** SEM images of Al-PyDC powder obtained from conventional reflux method, and single crystal obtained from the crystal synthesis method.

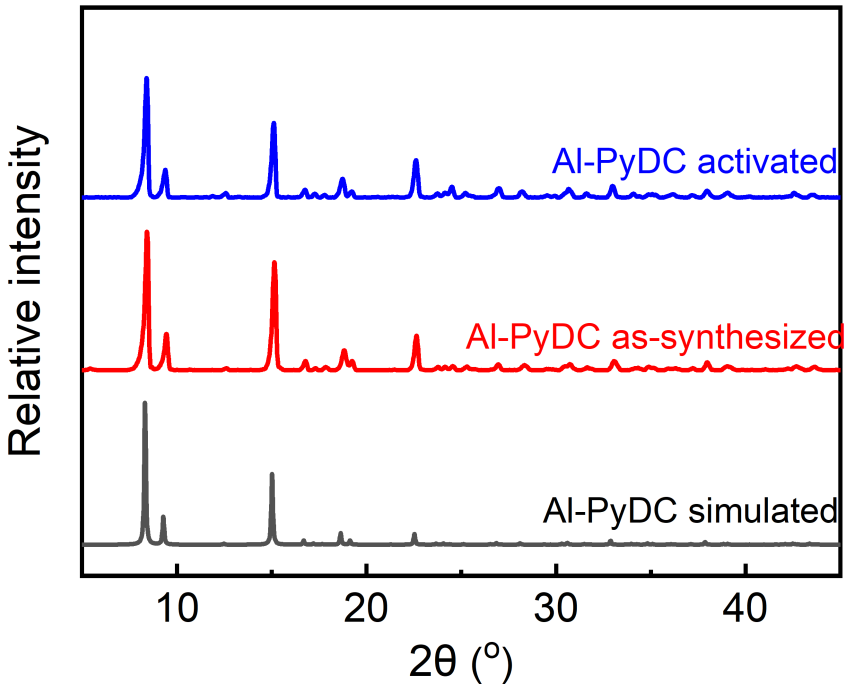


**Supplementary Fig. 2 PXRD patterns.** The calculated PXRD pattern from the model structure of Al-PyDC and PXRD patterns of as-synthesized Al-PyDC, activated Al-PyDC.

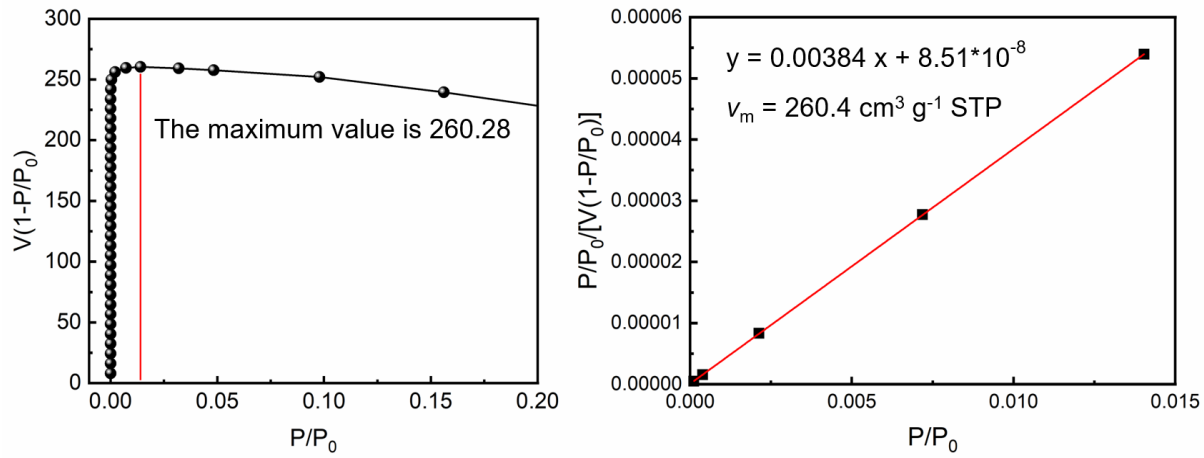


**Supplementary Fig. 3 Fit curves.** Al-PyDC BET specific surface area fitting.

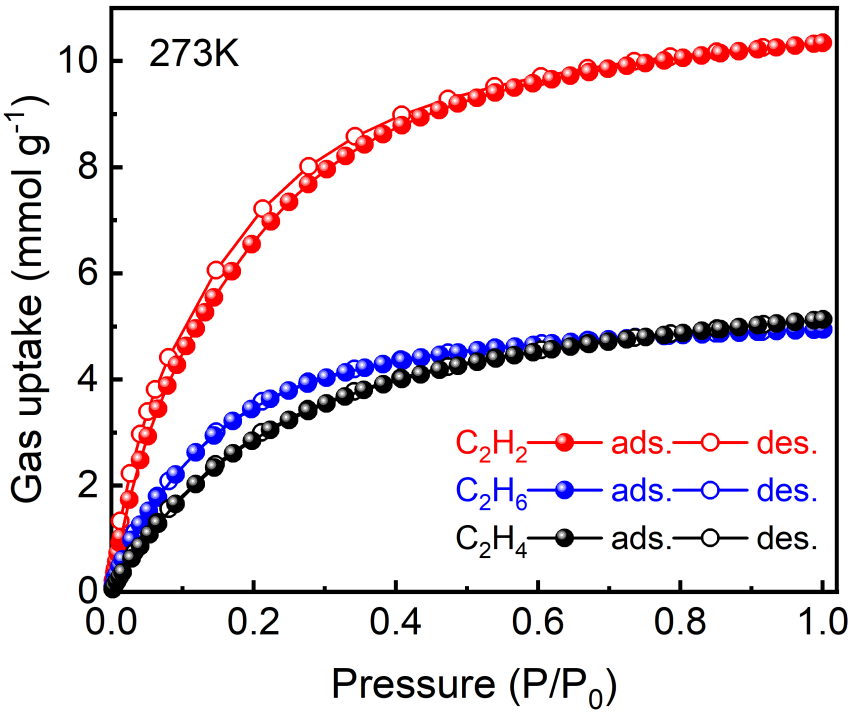


**Supplementary Fig. 4 $C_2$ adsorption**. Adsorption isotherms of $C_2H_2$ (red), $C_2H_6$ (blue) and $C_2H_4$ (black) for Al-PyDC at 273 K.

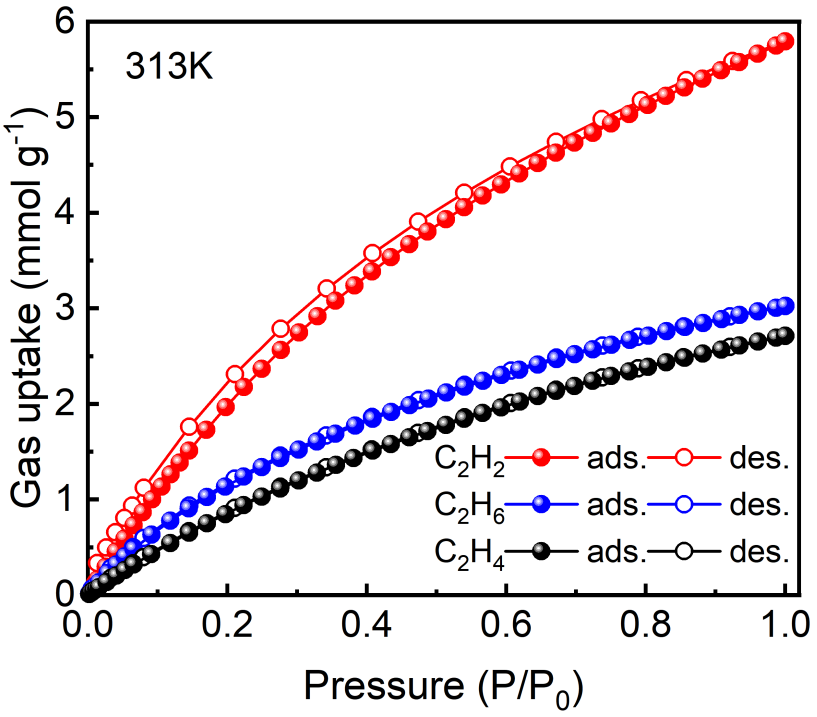


**Supplementary Fig. 5 $C_2$ adsorption**. Adsorption isotherms of $C_2H_2$ (red), $C_2H_6$ (blue) and $C_2H_4$ (black) for Al-PyDC at **a** 296 K and **b** 313 K.

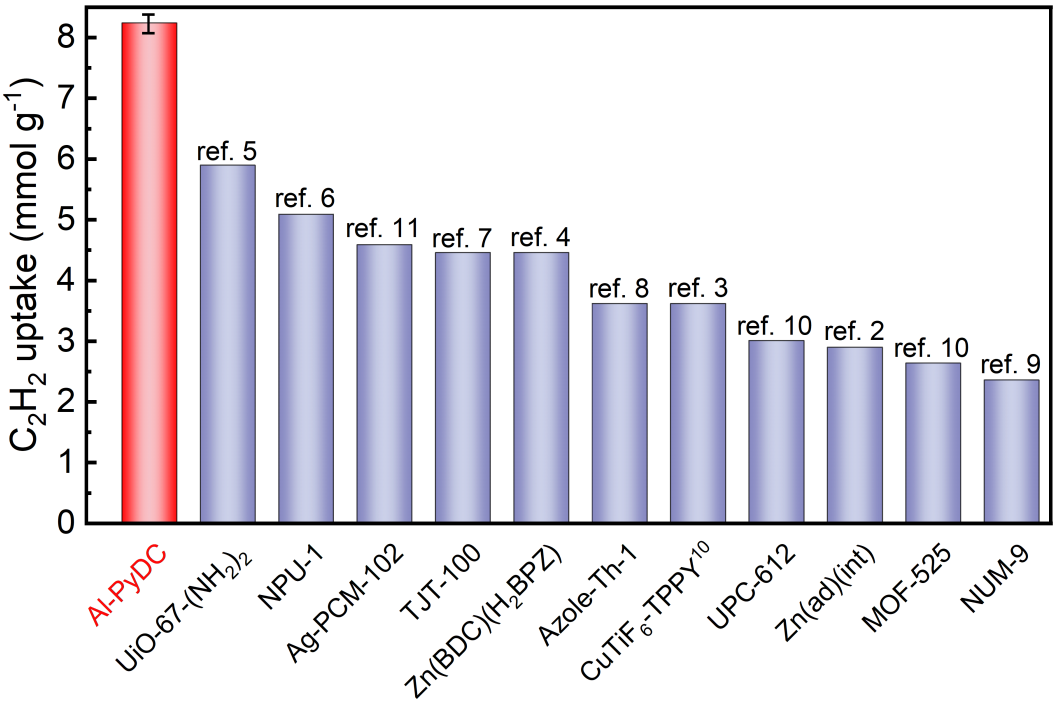


**Supplementary Fig. 6 Comparison of adsorption capacity.** Comparison of $C_2H_2$ uptake for Al-PyDC (the averaged value was obtained from five independent tests, and the error bar is the standard deviation) with the indicated benchmark MOFs at ambient conditions.

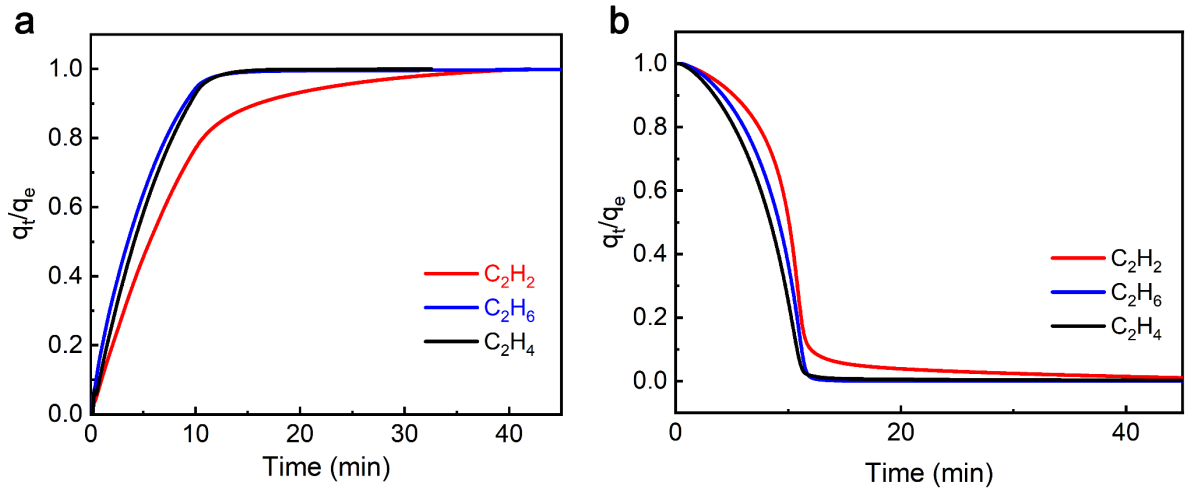


**Supplementary Fig. 7 Kinetics profiles. a** Adsorption kinetics profiles of $C_2H_2$ (red), $C_2H_6$ (blue) and $C_2H_4$ (black) for activated Al-PyDC at 296 K and 1 bar. **b** Desorption kinetics profiles of $C_2H_2$ (red), $C_2H_6$ (blue) and $C_2H_4$ (black) for saturated Al-PyDC at 296 K and $10^{-5}$ bar. $q_t/q_e$ represents the gravimetric uptake/total equilibrium gravimetric uptake (at 1 bar), indicating the gas sorption rate of materials.

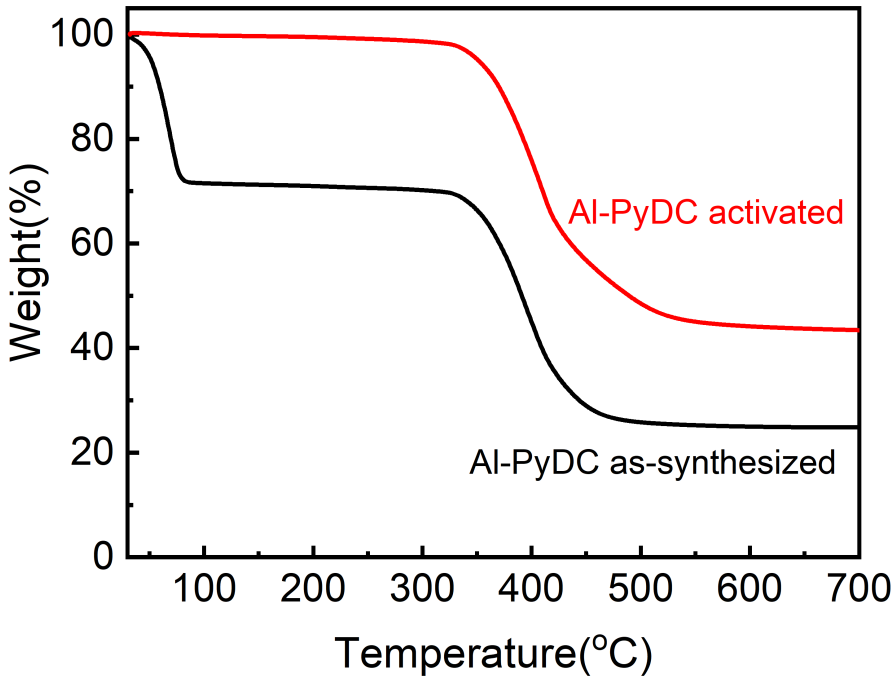


**Supplementary Fig. 8 TGA.** TGA analysis curve of as-synthesized (black) and activated (red) Al-PyDC. The data were collected under 5 K $min^{-1}$ of heating rate and 30 mL $min^{-1}$ $N_2$ flow.

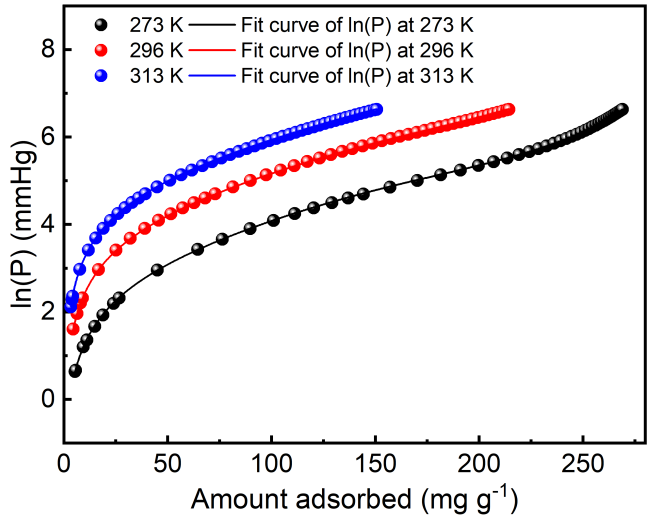


| Equation | y=ln(x)+1/k*(a0+a1*x+a2*x^2+a3*x^3 +a4*x^4+a5*x^5)+(b0+b1*x+b2*x^2) | |
|---|---|---|
| Adj. R-suqre | 0.99999 | |
| | Value | Standard Erro |
| a0* | -4273.31733 | 10.4357 |
| a1* | 4.99444 | 0.24812 |
| a2* | -0.02379 | 0.00227 |
| a3* | 1.19E-04 | 2.15E-05 |
| a4* | -8.38E-07 | 8.87E-08 |
| a5* | 1.83E-09 | 1.30E-10 |

**Supplementary Fig. 9 Fit curves.** Virial fitting of the $C_2H_2$ adsorption isotherms for Al-PyDC.

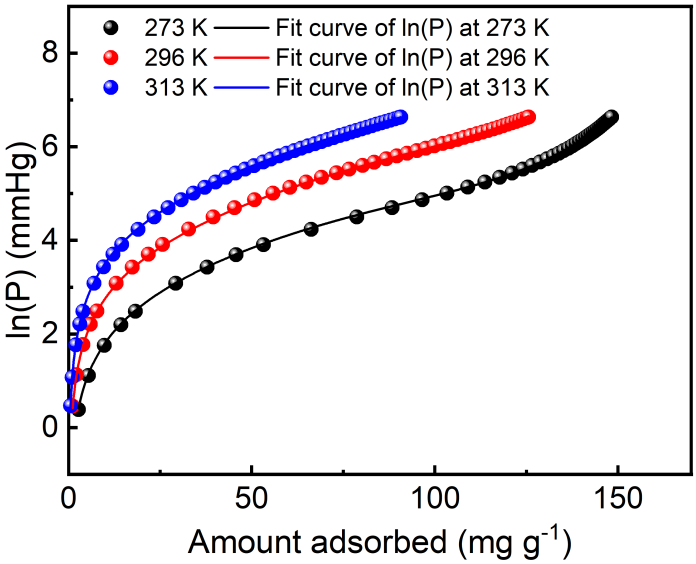


| Equation | y=ln(x)+1/k*(a0+a1*x+a2*x^2+a3*x^3 +a4*x^4+a5*x^5)+(b0+b1*x+b2*x^2) | |
|---|---|---|
| Adj. R-suqre | 0.99999 | |
| | Value | Standard Erro |
| a0* | -3619.84812 | 23.43929 |
| a1* | -0.55603 | 0.94057 |
| a2* | -0.05059 | 0.015 |
| a3* | 5.90E-04 | 2.40E-04 |
| a4* | -7.62E-06 | 1.76E-06 |
| a5* | 3.33E-08 | 4.65E-09 |

**Supplementary Fig. 10 Fit curves.** Virial fitting of the $C_2H_6$ adsorption isotherms for Al-PyDC.

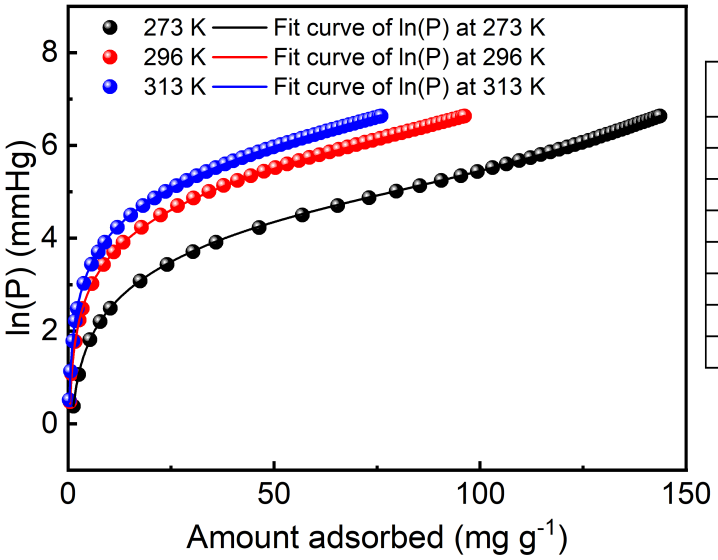


| Equation | y=ln(x)+1/k*(a0+a1*x+a2*x^2+a3*x^3 +a4*x^4+a5*x^5)+(b0+b1*x+b2*x^2) | |
|---|---|---|
| Adj. R-suqre | 0.99999 | |
| | Value | Standard Erro |
| a0* | -3375.76244 | 16.39543 |
| a1* | 0.95312 | 0.85817 |
| a2* | -0.03577 | 0.01177 |
| a3* | -7.38E-04 | 2.00E-04 |
| a4* | 6.60E-06 | 1.61E-06 |
| a5* | -1.70E-08 | 4.56E-09 |

**Supplementary Fig. 11 Fit curves.** Virial fitting of the $C_2H_4$ adsorption isotherms for Al-PyDC.

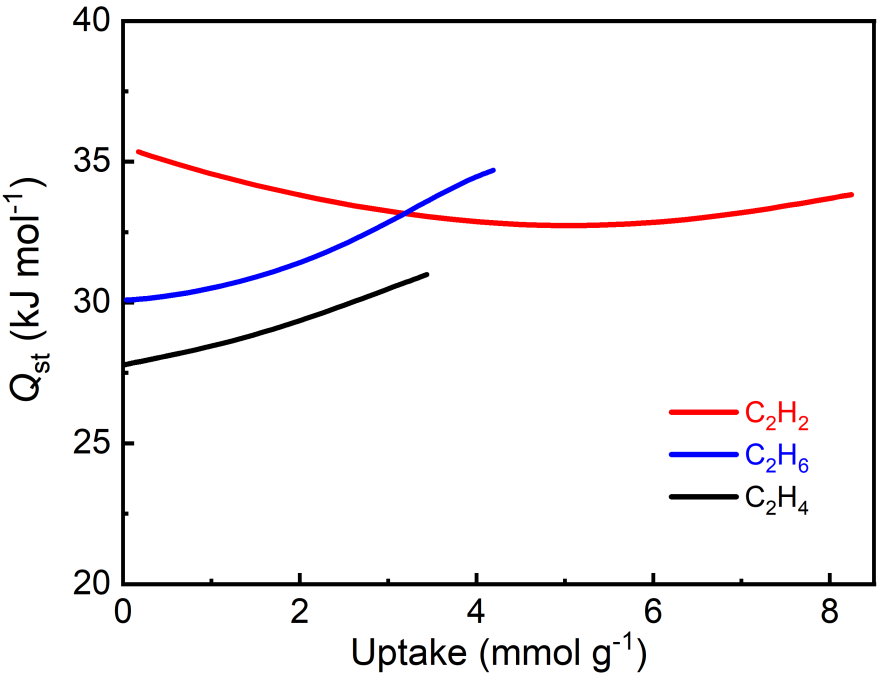


**Supplementary Fig. 12 $Q_{st}$.** The $Q_{st}$ of $C_2H_2$, $C_2H_6$ and $C_2H_4$ for Al-PyDC.

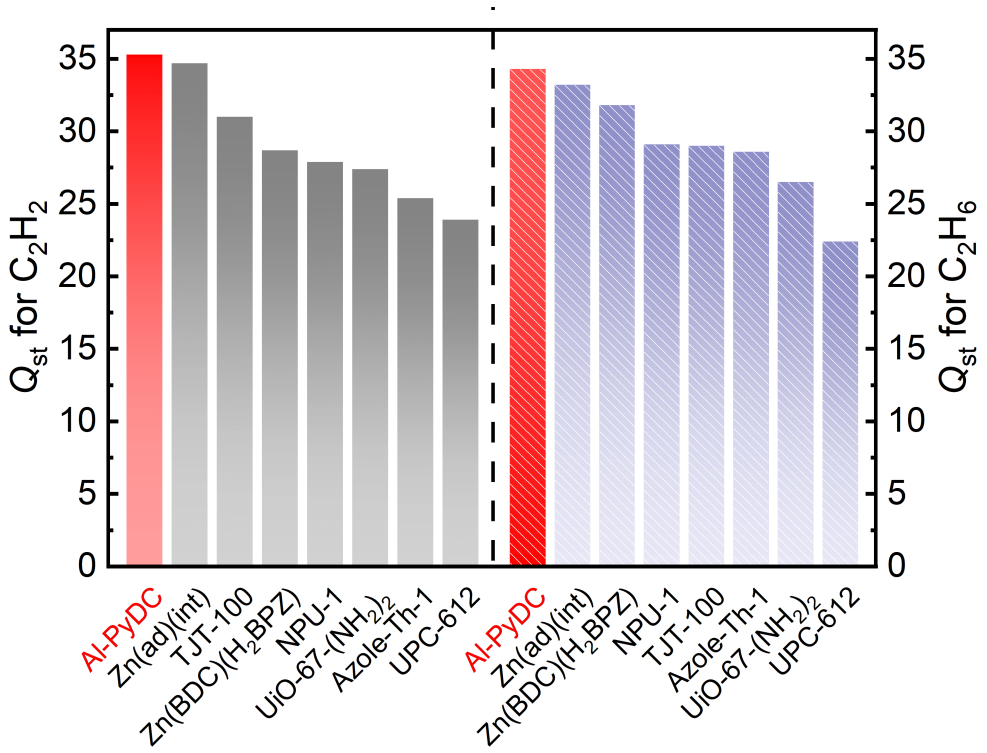


**Supplementary Fig. 13 Comparison of maximum $Q_{st}$.** The comparison of maximum $Q_{st}$ for $C_2H_2$ and $C_2H_6$.

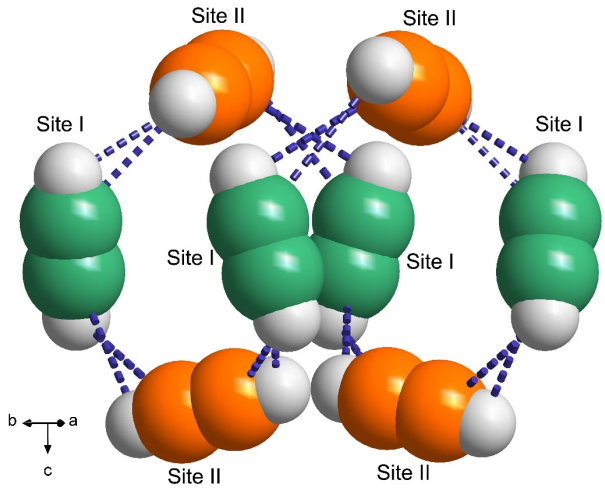


**Supplementary Fig. 14 Binding sites.** The $C_2H_2$ cluster in $C_2H_2$-loaded Al-PyDC determined by SCXRD analysis. The Al-PyDC framework is omitted for clarity.

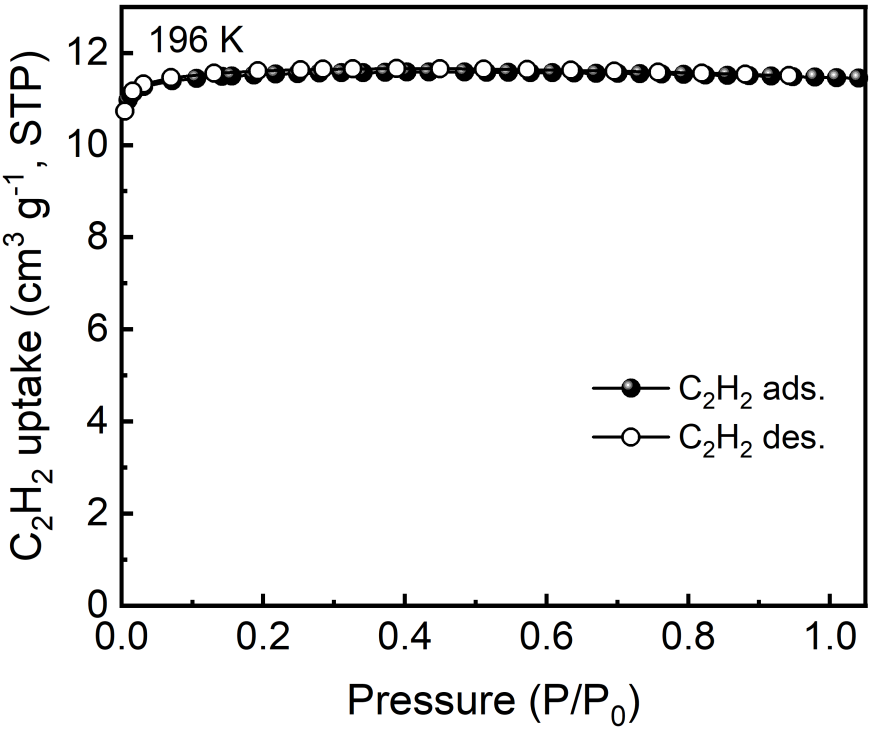


**Supplementary Fig. 15 $C_2H_2$ sorption.** $C_2H_2$ sorption isotherms of Al-PyDC at 196 K.

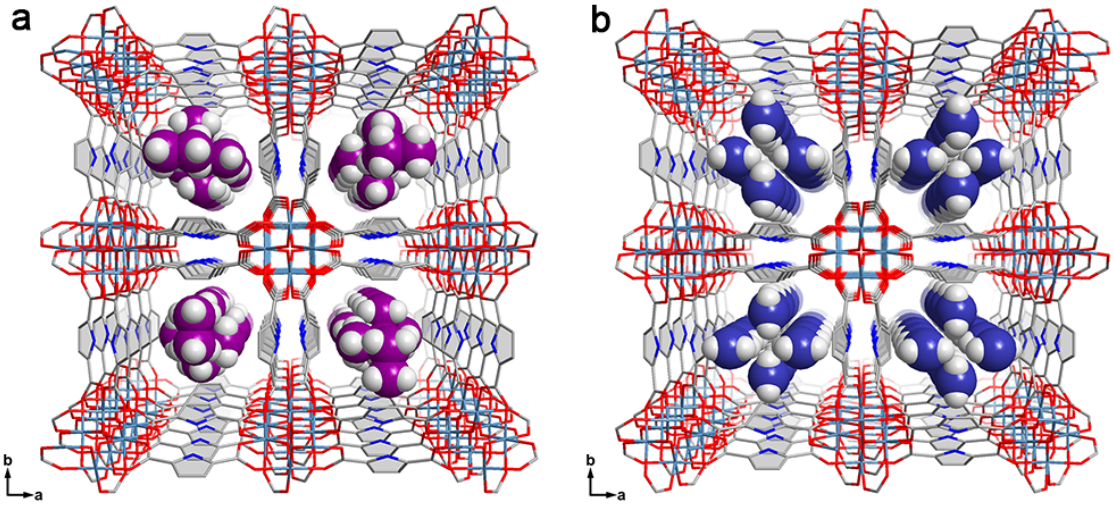


**Supplementary Fig. 16 Binding sites.** The SCXRD structures of **a** $C_2H_6$-loaded and **b** $C_2H_4$-loaded Al-PyDC, viewed along the *c* axis.

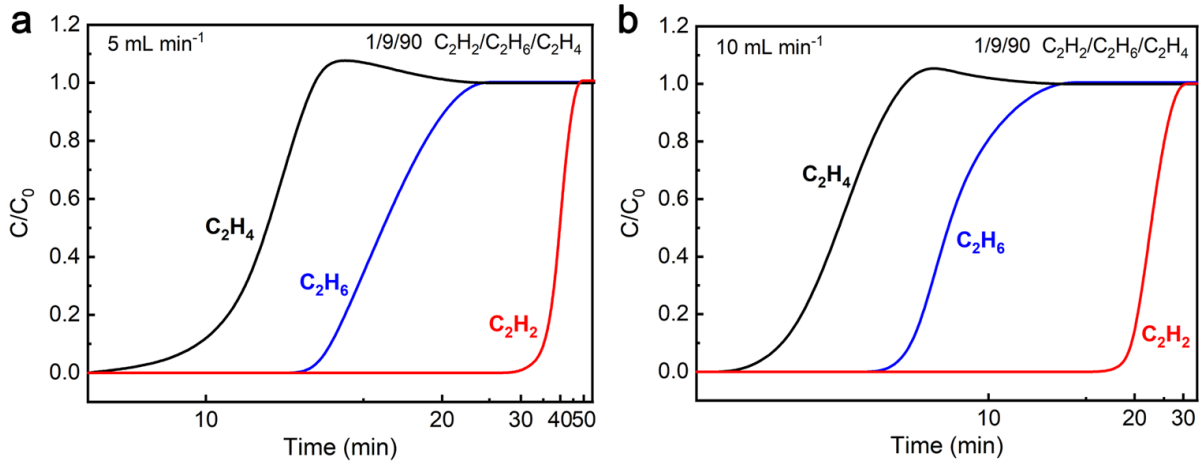


**Supplementary Fig. 17 Breakthrough curves.** Experimental column breakthrough curves for $C_2H_2/C_2H_6/C_2H_4$ (1/9/90) mixture with a total flow of **a** 5 mL $min^{-1}$ and **b** 10 mL $min^{-1}$ in an absorber bed packed with Al-PyDC at 296 K and 1 bar.

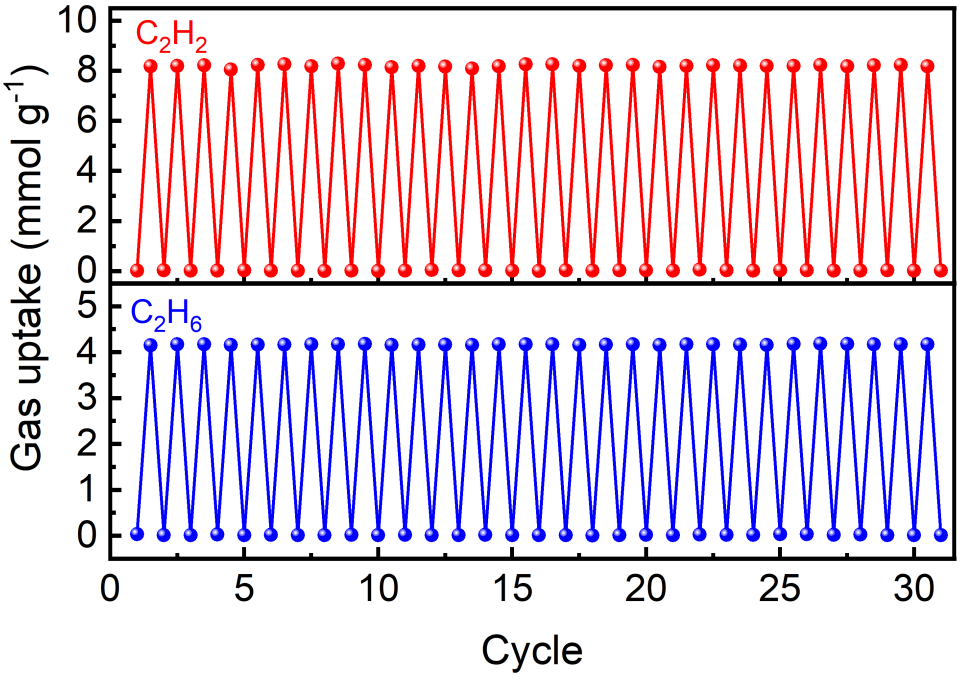


**Supplementary Fig. 18 Recyclability.** The repeated adsorption-desorption cycles of Al-PyDC for $C_2H_2$ and $C_2H_6$ sorption at 296 K between the pressure of 1 bar and 0.001 bar.

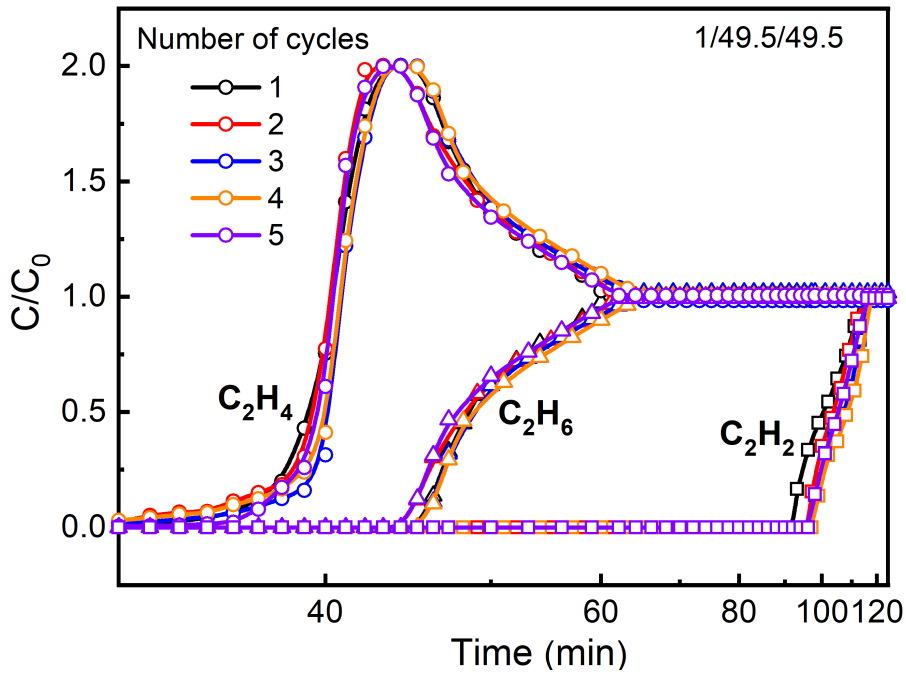


**Supplementary Fig. 19 Recyclability.** The five repeated separation cycles of breakthrough experiments on Al-PyDC for the 1/49.5/49.5 $C_2H_2/C_2H_6/C_2H_4$ mixture.

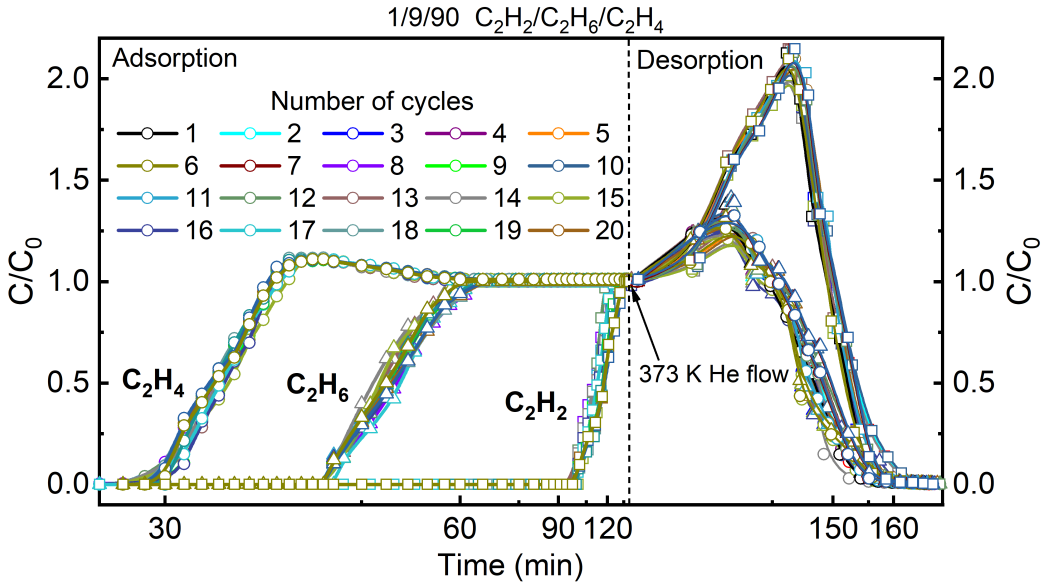


**Supplementary Fig. 20 Recyclability.** The twenty repeated adsorption-desorption cycles of breakthrough experiments on Al-PyDC for the 1/9/90 $C_2H_2/C_2H_6/C_2H_4$ mixture.

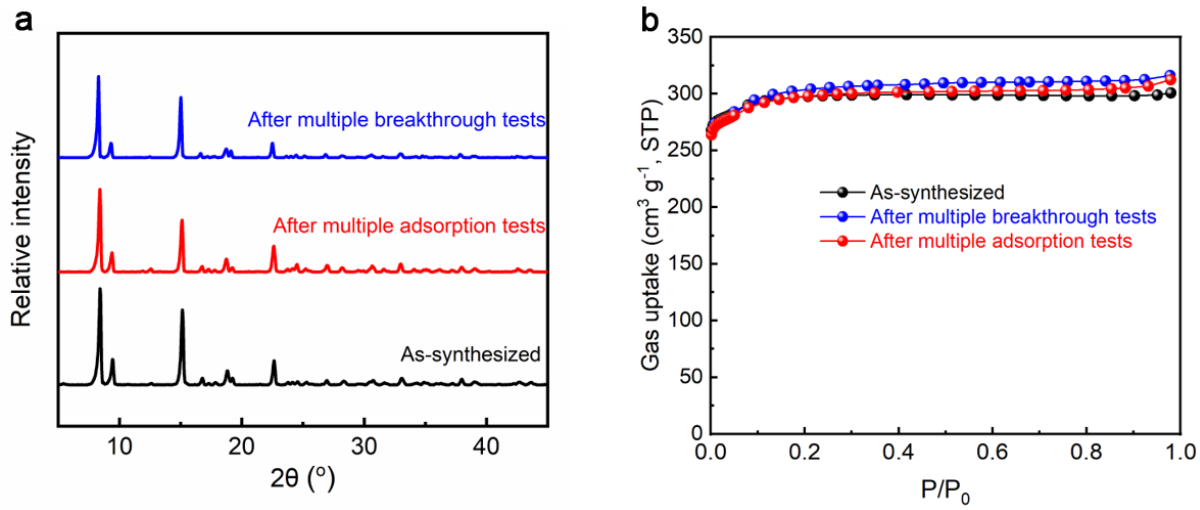


**Supplementary Fig. 21 Recyclability. a** PXRD patterns of Al-PyDC samples after multiple adsorption and breakthrough tests. **b** $N_2$ adsorption isotherms at 77 K of Al-PyDC after multiple adsorption and breakthrough tests.

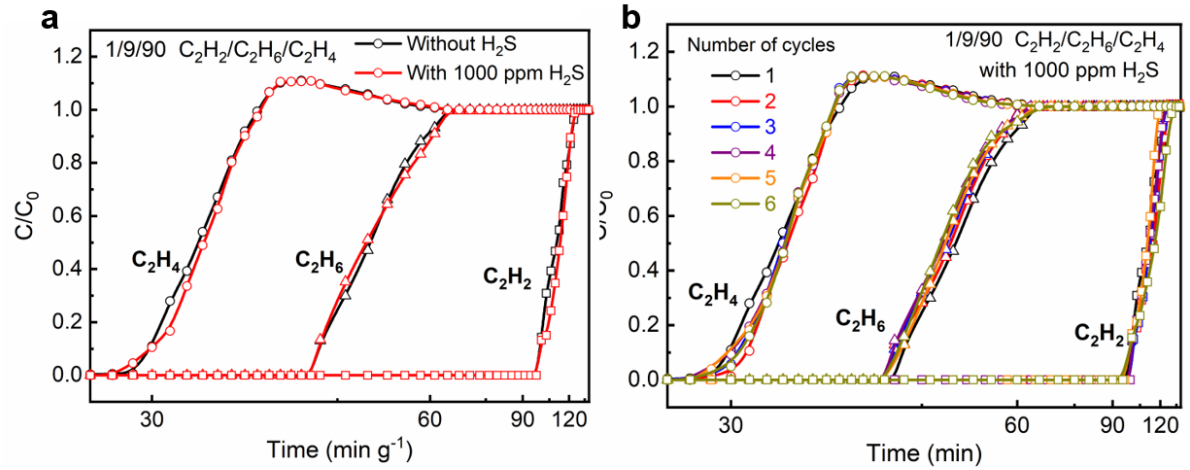


**Supplementary Fig. 22 Stability and recyclability. a** Experimental breakthrough curves of Al-PyDC for 1/9/90 $C_2H_2/C_2H_6/C_2H_4$ mixture with 1000 ppm $H_2S$. **b** The cycling tests of Al-PyDC for 1/9/90 $C_2H_2/C_2H_6/C_2H_4$ mixture with 1000 ppm $H_2S$.

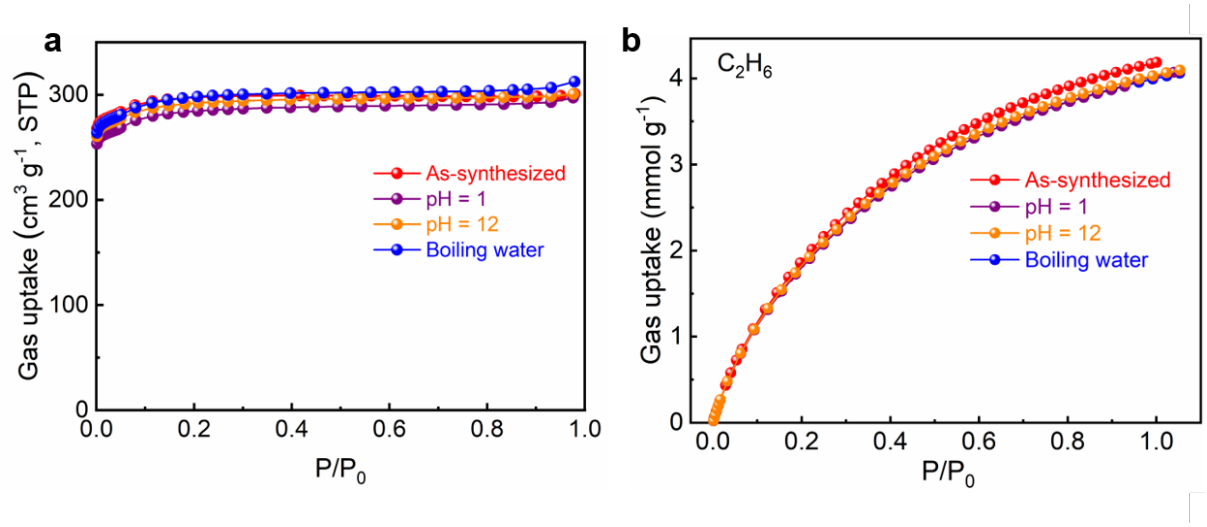


**Supplementary Fig. 23 Chemical stability. a** $N_2$ and **b** $C_2H_6$ adsorption isotherms of Al-PyDC samples after treatment with different conditions at 77 K and 296 K, respectively.

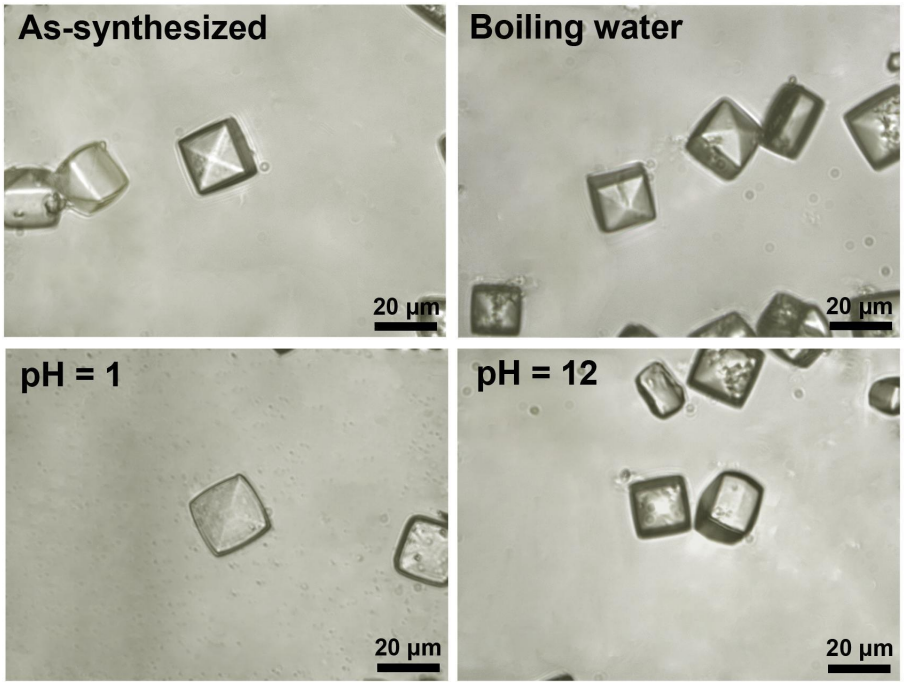


**Supplementary Fig. 24 Optical microscope images.** Optical microscope images of Al-PyDC crystal after treatment under different conditions.

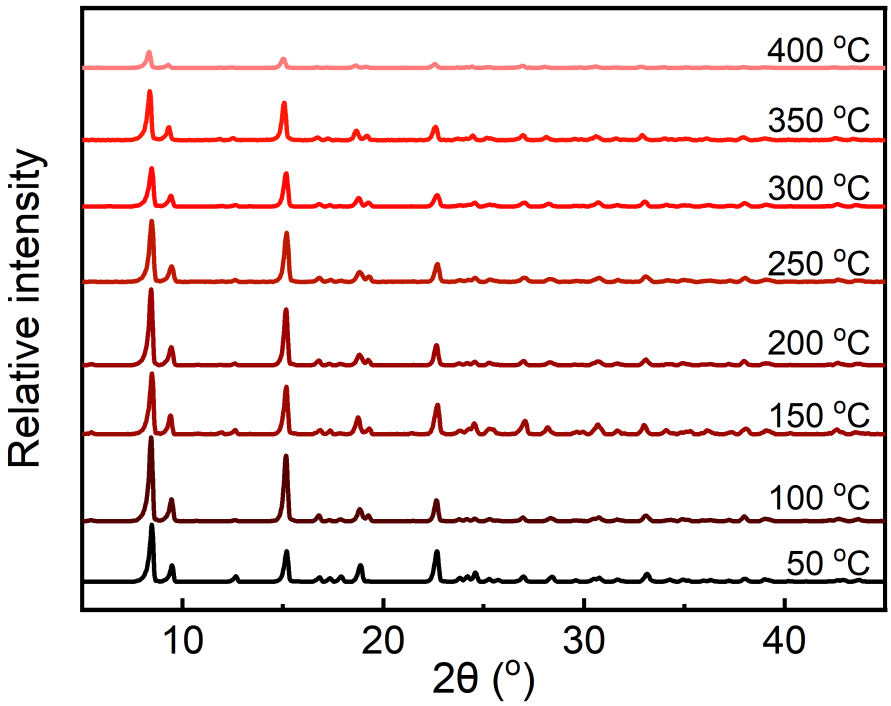


**Supplementary Fig. 25 Thermal stability.** Variable-temperature PXRD patterns for Al-PyDC.

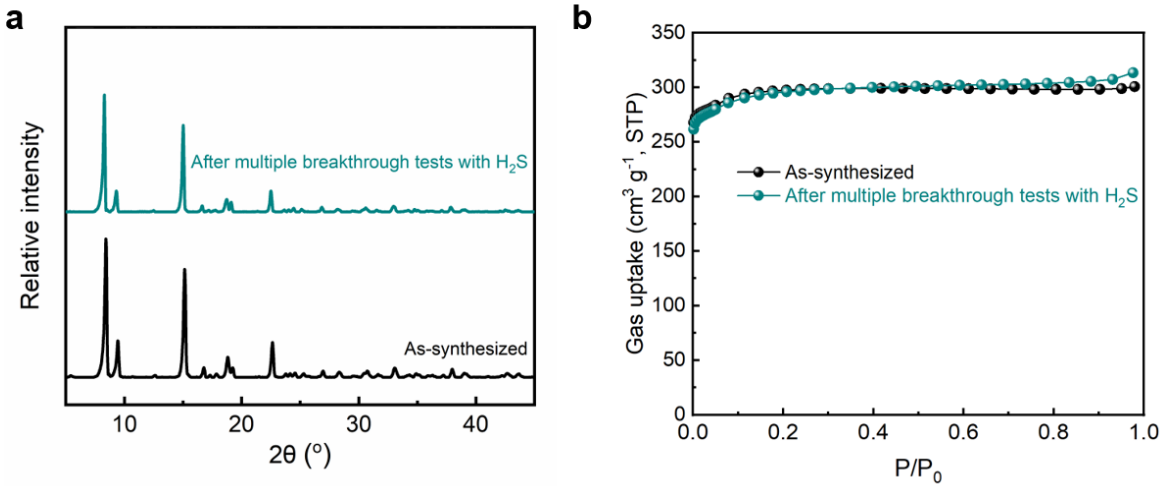


**Supplementary Fig. 26 Stability. a** PXRD patterns of Al-PyDC samples after multiple breakthrough tests for 1/9/90 $C_2H_2/C_2H_6/C_2H_4$ mixture with 1000 ppm $H_2S$. **b** $N_2$ adsorption isotherms at 77 K of Al-PyDC after multiple breakthrough tests for 1/9/90 $C_2H_2/C_2H_6/C_2H_4$ mixture with 1000 ppm $H_2S$.

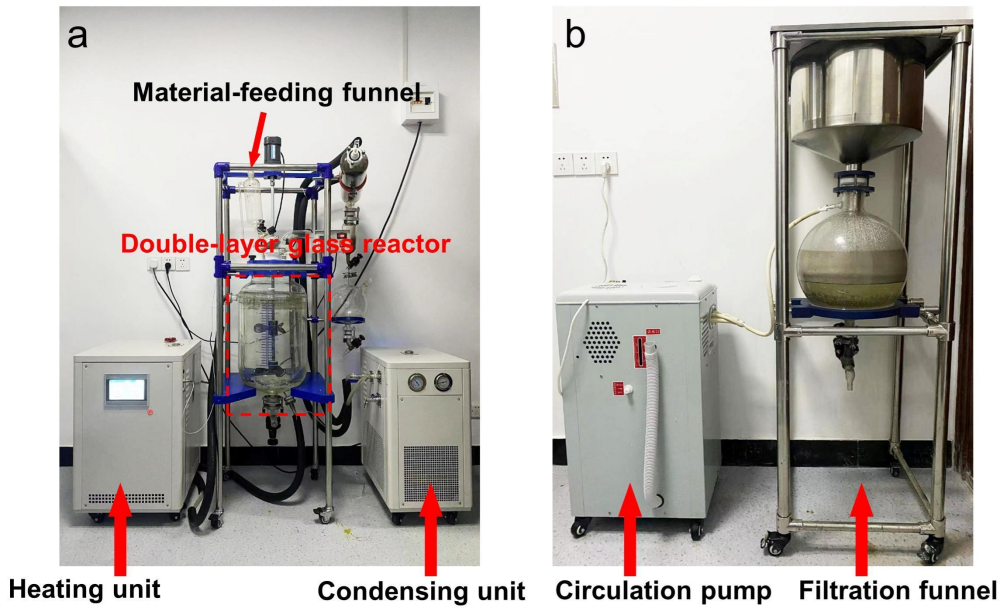


**Supplementary Fig. 27 Synthesis unit. a** The large scale synthesis vessel consists of a heating unit, a condensing unit, a material-feeding funnel and a 30 L double glazed reactor, where the temperature of the reactor is controlled by heating the silicone oil between the glass interlayers. **b** The 20L filtration funnel with circulation pump.

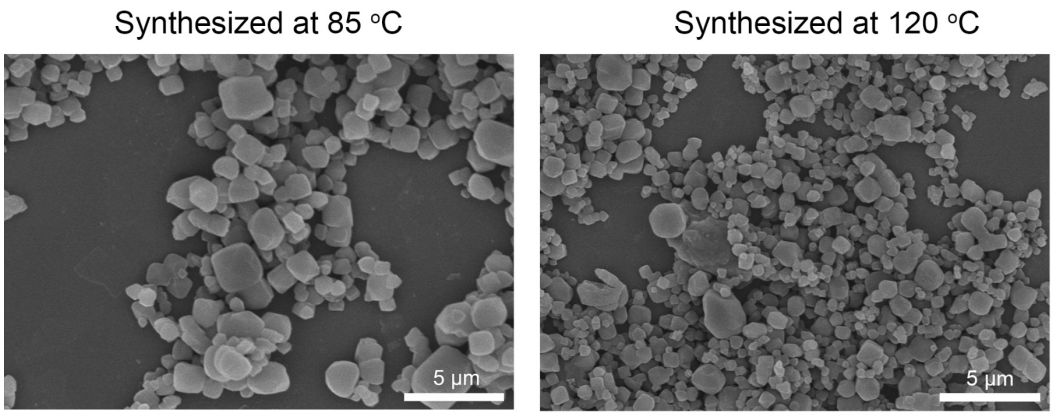


**Supplementary Fig. 28 SEM images.** (left) The SEM images of large-scale sample synthesized at low temperature (85 °C), and (right) the powder sample synthesized at 120 °C according to the literature[18].

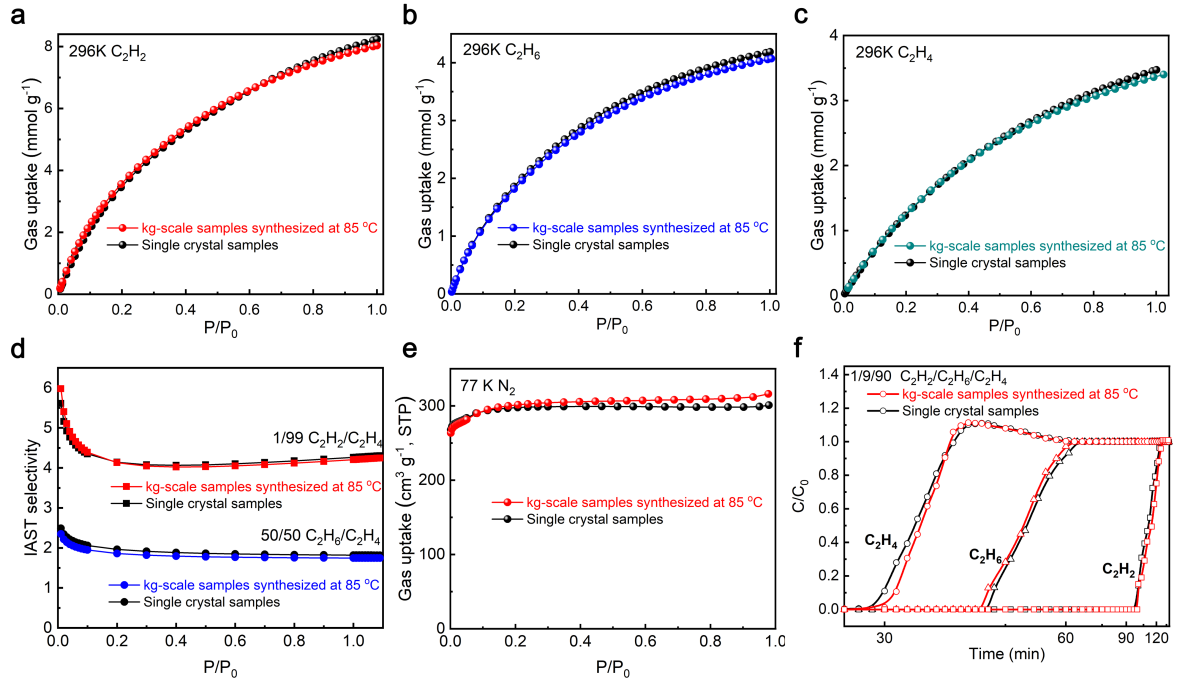


**Supplementary Fig. 29 Scalability.** Comparison of **a-c** $C_2$ gas adsorption at 296 K, **d** $N_2$ adsorption at 77 K, **e** IAST selectivity and **f** breakthrough experiment curves of kg-scale Al-PyDC sample synthesized at low temperature of 85 °C with those obtained from single crystal sample.

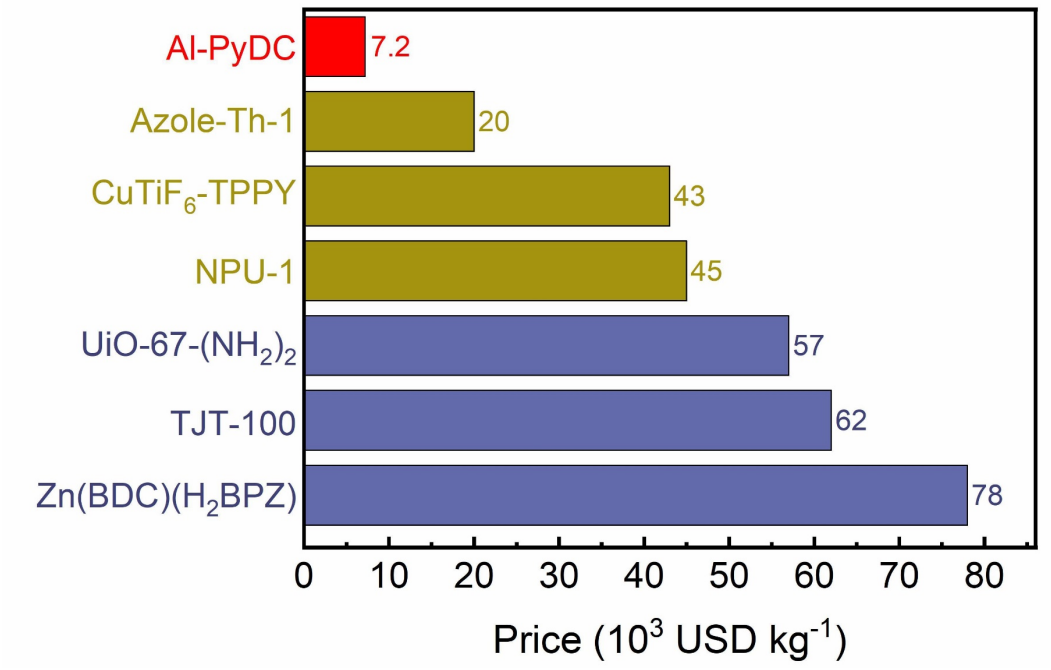


**Supplementary Fig. 30 Economic feasibility.** Comparison of the price of organic ligands for best-performing MOF materials. The prices were inquired by Bidepharm (China) or other companies. Note that: the values of ligand price are used only for the qualitative comparison purpose.

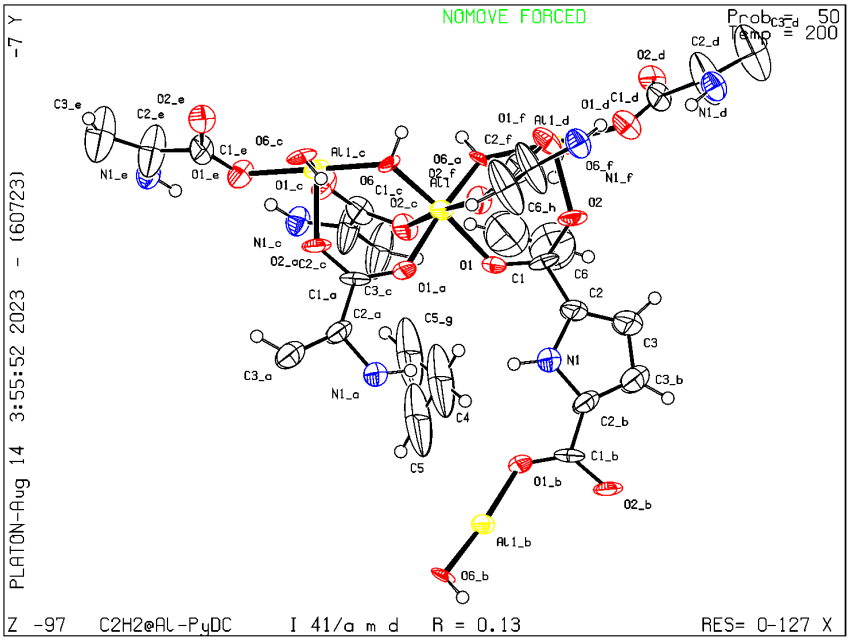


**Supplementary Fig. 31 ORTEP.** ORTEP drawing of the $C_2H_2$@Al-PyDC, produced by the checkCIF report of the International Union of Crystallography. CCDC deposit number 2242152.

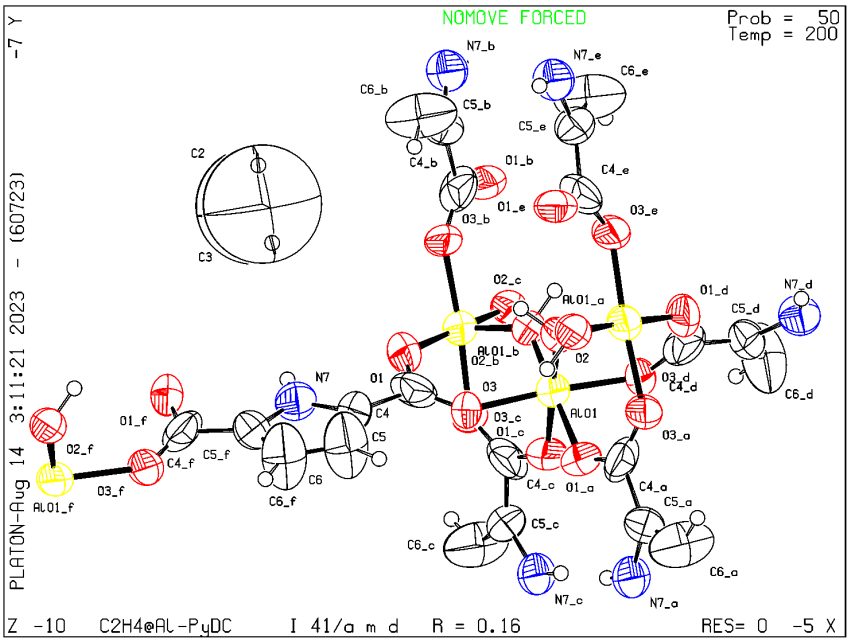


**Supplementary Fig. 32 ORTEP.** ORTEP drawing of the $C_2H_4$@Al-PyDC, produced by the checkCIF report of the International Union of Crystallography. CCDC deposit number 2242153.

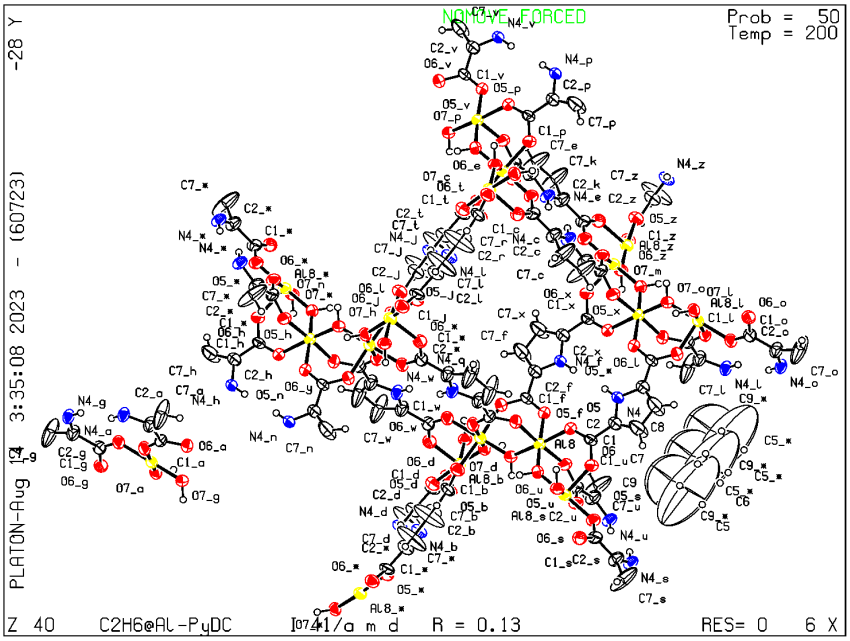


**Supplementary Fig. 33 ORTEP.** ORTEP drawing of the $C_2H_6$@Al-PyDC, produced by the checkCIF report of the International Union of Crystallography. CCDC deposit number 2242154.

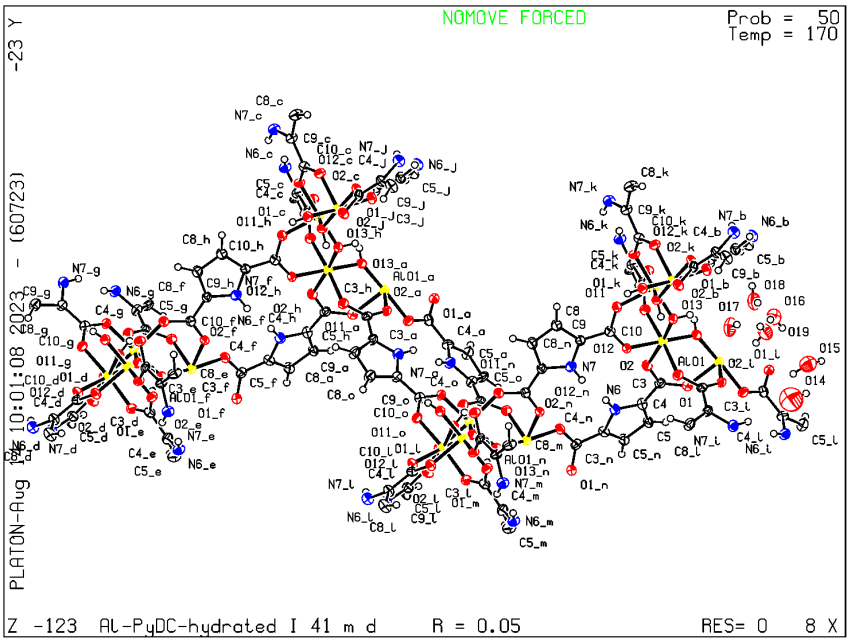


**Supplementary Fig. 34 ORTEP.** ORTEP drawing of the Al-PyDC-hydrated, produced by the checkCIF report of the International Union of Crystallography. CCDC deposit number 2242155.

**Disclaimer**: Certain commercial suppliers are identified in this paper to foster understanding. Such identification does not imply recommendation or endorsement by the National Institute of Standards and Technology, nor does it imply that the materials or equipment identified are necessarily the best available for the purpose.

## Supplementary References


1. Zhang, X. et al. Selective ethane/ethylene separation in a robust microporous hydrogen-bonded organic framework, *J. Am. Chem. Soc.* **142**, 633−640 (2020).

2. Ding, Q. et al. One-step ethylene purification from ternary mixtures in a metal−organic framework with customized pore chemistry and shape. *Angew. Chem. Int. Ed.* **61**, e202208134 (2022).

3. Zhang, P. et al. Synergistic binding sites in a hybrid ultramicroporous material for one-step ethylene purification from ternary $C_2$ hydrocarbon mixtures. *Sci. Adv.* **8**, eabn9231 (2022).

4. Wang, G.-D. et al. One-step $C_2H_4$ purification from ternary $C_2H_6/C_2H_4/C_2H_2$ mixtures by a robust metal-organic framework with customized pore environment. *Angew. Chem. Int. Ed.* **61**, e202205427 (2022).

5. Gu, X.-W. et al. Immobilization of Lewis basic sites into a stable ethane-selective MOF enabling one-step separation of ethylene from a ternary mixture. *J. Am. Chem. Soc.* **144**, 2614−2623 (2022).

6. Zhu, B. et al. Pore engineering for one-step ethylene purification from a three-component hydrocarbon mixture. *J. Am. Chem. Soc.* **143**, 1485−1492 (2021)

7. Hao, H.-G. et al. Simultaneous trapping of $C_2H_2$ and $C_2H_6$ from a ternary mixture of $C_2H_2/C_2H_4/C_2H_6$ in a robust metal−organic framework for the purification of $C_2H_4$. *Angew. Chem. Int. Ed.* **57**, 16067−160711 (2018).

8. Xu, Z. et al. A robust Th-azole framework for highly efficient purification of $C_2H_4$ from a $C_2H_4/C_2H_2/C_2H_6$ mixture. *Nat. Commun.* **11**, 3163 (2020).

9. Yang, S.-Q. et al. Efficient purification of ethylene from $C_2$ hydrocarbons with an $C_2H_6/C_2H_2$-selective metal−organic framework. *ACS Appl. Mater. Interfaces* **13**, 962−969 (2021).

10. Wang, Y. et al. One-step ethylene purification from an acetylene/ethylene/ethane ternary mixture by cyclopentadiene cobalt-functionalized metal−organic frameworks. *Angew. Chem. Int. Ed.* **60**, 11350−11358 (2021).

11. Sikma, R. E. et al. Low-valent metal ions as MOF pillars: a new route toward stable and multifunctional MOFs. *J. Am. Chem. Soc.* **143**, 13710−13720 (2021).

12. Qian, X. et al. Structure stability of metal-organic framework MIL-53 (Al) in aqueous solutions. *Int. J. Hydrogen Energy.* **38**, 16710−16715 (2013).

13. Huang, Y., Qin, W., Li, Z. & Li, Y. Enhanced stability and $CO_2$ affinity of a UiO-66 type metal−organic framework decorated with dimethyl groups. *Dalton Trans.* **41**, 9283−9285 (2012).

14. Park, K. S. et al. Exceptional chemical and thermal stability of zeolitic imidazolate frameworks. *Proc. Natl. Acad. Sci.* **103**, 10186−10191 (2006).

15. Wang, K., Li, Y., Xie, L.-H., Li, X. & Li, J.-R. Construction and application of base-stable MOFs: a critical review. *Chem. Soc. Rev.* **51**, 6417−6441 (2022).

16. Feng, D. et al. Kinetically tuned dimensional augmentation as a versatile synthetic route towards robust metal−organic frameworks. *Nat. Commun.* **5**, 5723 (2014).

17. Wang, B. et al. Highly stable Zr(IV)-based metal−organic frameworks for the detection and removal of antibiotics and organic explosives in water. *J. Am. Chem. Soc.* **138**, 6204−6216 (2016).

18. Cho, K. H. et al. Rational design of a robust aluminum metal-organic framework for multi-purpose water-sorption-driven heat allocations. *Nat. Commun.* **11**, 5112 (2020).